Onset of Random Matrix Behavior in Scrambling Systems

HARIBYAN ANADA HENKER EZUKA

Stanford Institute for Theoretical Physics, Stanford University, Stanford, CA 94305, USA

Yukawa Institute for Theoretical Physics, Kyoto University, Kyoto 606-8502, Japan

The Hakubi Center for Advanced Research, Kyoto University, Kyoto 606-8501, Japan

Department of Physics, University of Colorado, Boulder, Colorado 80309, USA

Department of Physics, Kyoto University, Kyoto 606-8502, Japan

diffusion time

universal

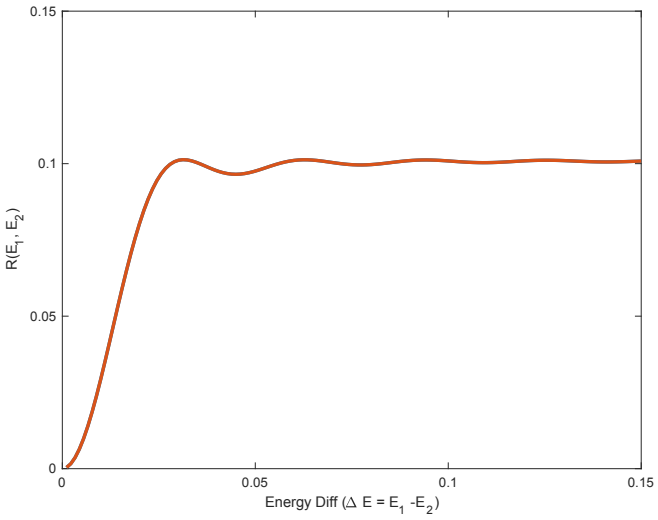
0.15
0.1
0.05
0
R(E1, E2)
0
0.05
0.1
0.15
Energy Diff (Δ E = E1 -E2)

not

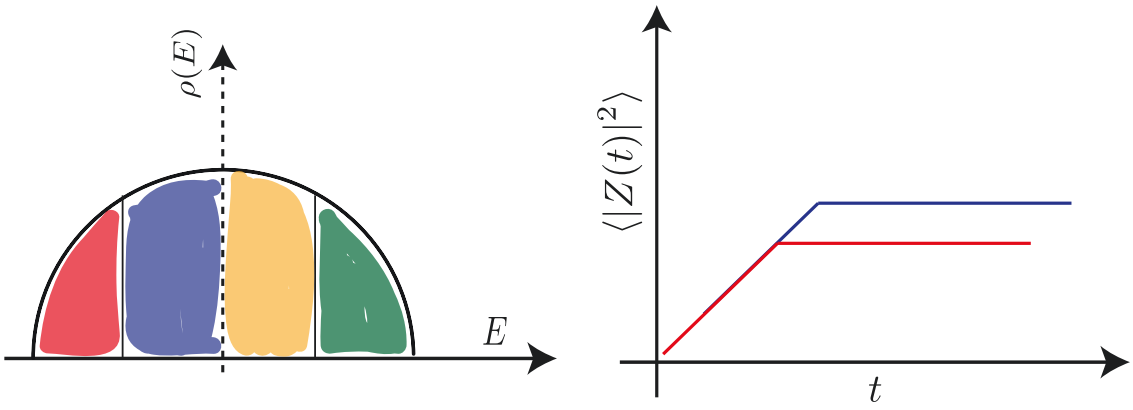
$\rho(E)$
E
$\langle |Z(t)|^2 \rangle$
t

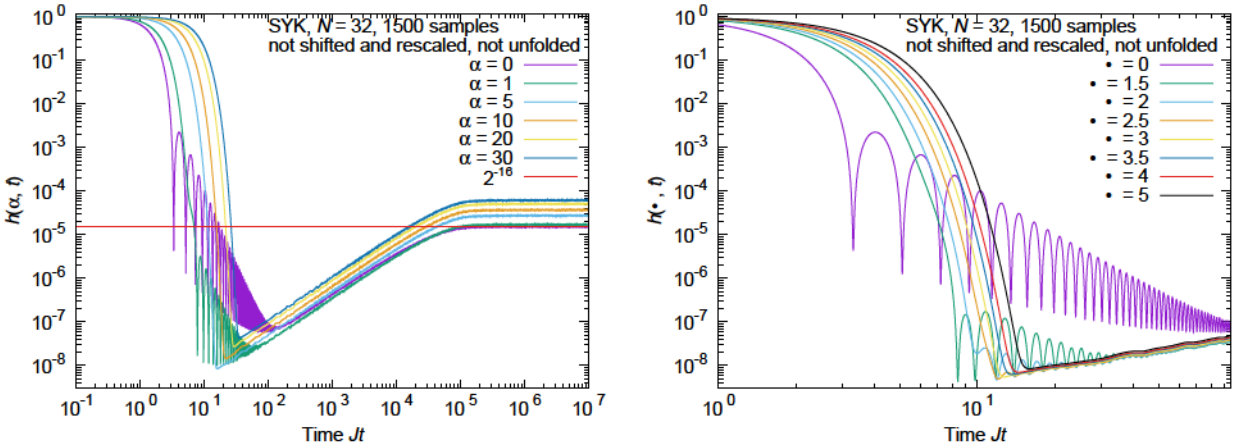

Figure 3: $h(\alpha, t) \equiv |Y(\alpha, t)|^2 / |Y(\alpha, t = 0)|^2$ at $N = 32$, with various values of α. Note that $g(t) = h(\alpha = 0, t)$.

which hides the onset of the ramp. This is visible in the $\alpha = 0$ curves where $h(t) = g(t)$ in Fig. 3. In Fig. 4 (using the optimal value of α) we can see that the ramp continues all the way down to the Gaussian envelope, and may well continue past it. This intersection time, which we call $t_{\rm min}$, gives an upper bound to the ramp time $t_{\rm ramp}$. In the data displayed the ramp extends down to a time $t_{\rm min}$ of order 10. The plateau time is of order 10^5 here, so this represents a ratio of 10^4 in time or energy scales. Note that there are only $2^{16} \sim 66\,000$ energy levels[12] in the spectrum so rigidity extends across an appreciable fraction of the entire spectrum![13] We should emphasize that as expected $t_{\rm min}$ is far less, over an order of magnitude here, than $t_{\rm dip}$.

It seems from the graph that the ramp probably extends somewhat further but is just being masked by the Gaussian envelope. For this finite value of N it is impossible to do better because an envelope that decays faster in time corresponds to a Gaussian filter that is broader in energy and extends closer to the edge of the spectrum, allowing more contamination from the sharp edge. But as N grows this effect goes away because the edges of the spectrum are at energies $\pm cN$ (even though the standard deviation of the energy is of order $\sqrt{N}$). The Gaussian filter lets in an edge signal in $\langle |Y(\alpha, t)|^2 \rangle$ of order $e^{-2\alpha(cN)^2 + 2s_0 N}/t^3$ where $s_0 N$ is the zero temperature entropy. The early time ramp signal

[12] After removing the two fold fermion parity degeneracy which is the only degeneracy present for $N = 32$ [50].

[13] Of course a precise comparison would require evaluating various numerical factors of order one.

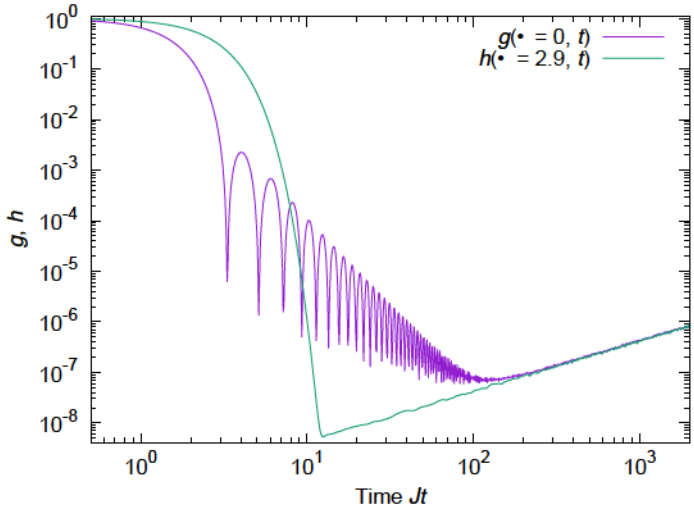

Figure 4: $g(t) = |Z(t)|^2/|Z(0)|^2$ and $h(\alpha, t) = |Y(\alpha, t)|^2/|Y(\alpha, t = 0)|^2$ with $\alpha = 2.9$ for $N = 32$, 1500 samples.

is of order one. So choosing α as small as $\frac{s_0}{c^2 N}$ is sufficient to mask the slope contribution from the edge. The Fourier transform of the Gaussian envelope decays $\sim e^{2s_\infty N - \frac{t^2}{4\alpha}}$ where $s_\infty N$ is the infinite temperature entropy. So an $\alpha \sim 1/N$ is small enough for the Gaussian envelope to become order one in a time of order one, allowing the study of t_{ramp} as short as order one. Thus this quantity provides a reliable definition of the Thouless time in SYK and other many-body systems with similar properties. The required N values may well be computationally prohibitive though.

We discuss our detailed algorithm for determining t_{min} in Appendix A.2. The oscillations in the data make this determination quite noisy. The values listed in Table 1 in the Appendix provide upper bounds for t_{ramp}. The best we can say about the N dependence is that it is weak. Power laws faster than N^1 and exponentials, with order one coefficients, are disfavored. A $\log N$ behavior would certainly be consistent.

To gain more experience we now examine a k- local model without a sharp edge in its density of states.

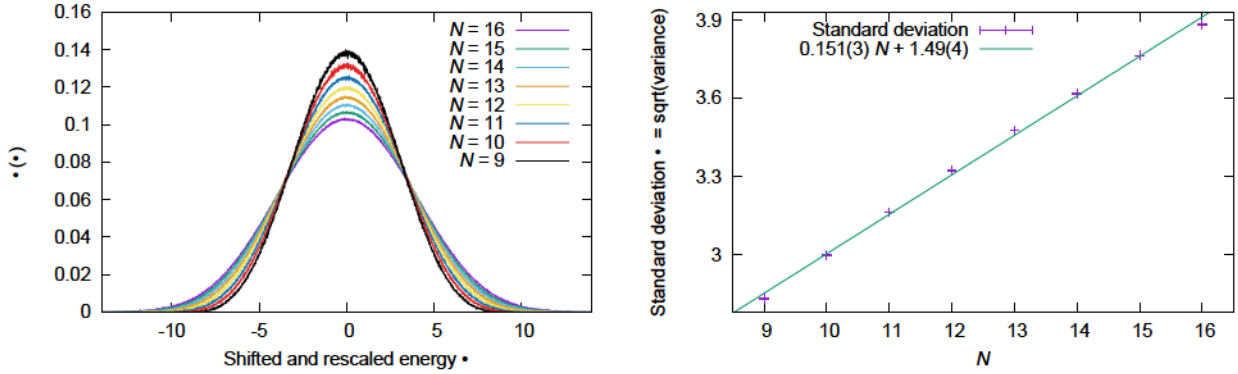

Figure 5: The density of shifted and renormalized eigenvalues for the 2-local RCQ model for $N = 9, 10, \ldots, 16$, and the averaged variance of eigenvalues with a straight line fit. $(2^{16-N} \times 100)$ samples have been used for each N.

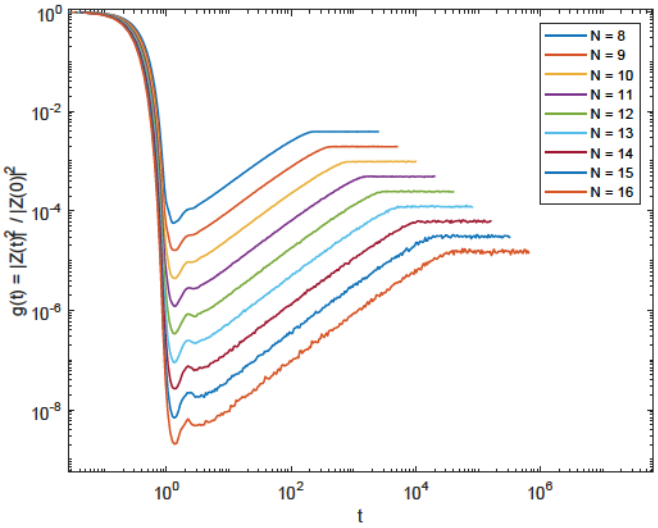

Figure 6: The spectral form factor for the k-local randomly coupled qubits (RCQ) with 8 to 16 qubits. We observe the Gaussian decay at the early times, follow by a 'bump', ramp and plateau.

mented with using YY^*. We were unable to isolate a sizable transition region to the ramp while excluding the bump. We do not understand its origin, unfortunately.

Nonetheless it is clear that the ramp begins early, at times between 2 and 5, increasing slowly with N. For $N = 16$ (see Fig. 7) the plateau time is about 10 000 times greater than the ramp time. The entire spectrum contains $2^{16} \sim 66\,000$ eigenvalues. So as in the

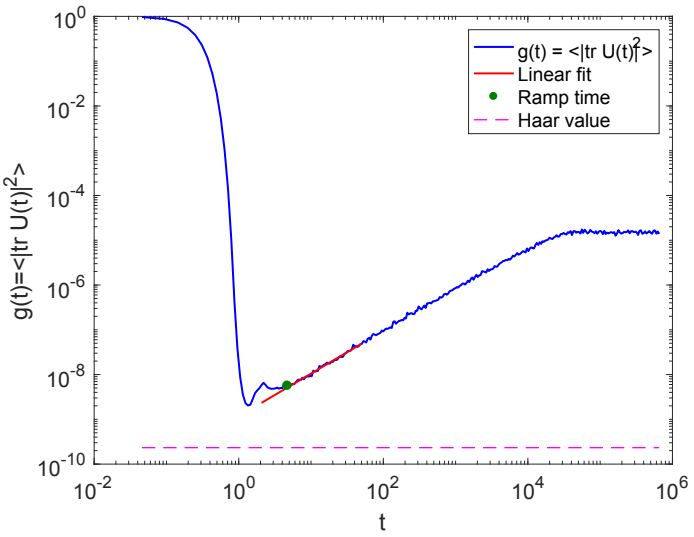
g(t) = <|tr U(t)|2>
Linear fit
Ramp time
Haar value
g(t)=<|tr U(t)|2>
t
10^0
10^-2
10^-4
10^-6
10^-8
10^-10
10^-2
10^0
10^2
10^4
10^6

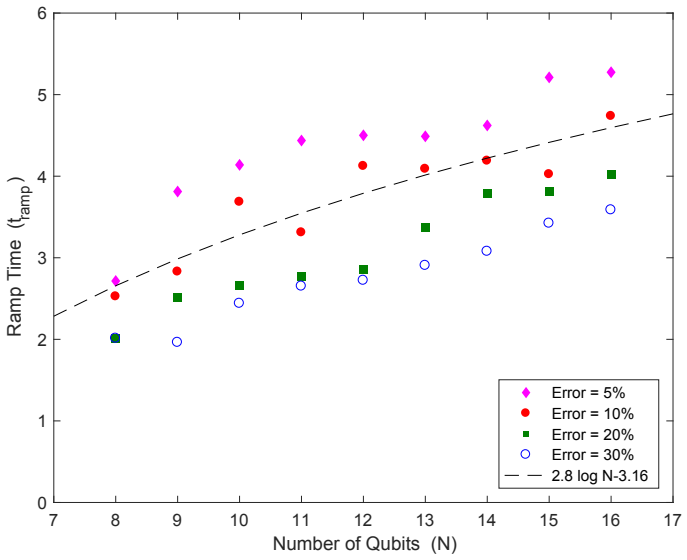
Ramp Time (t_{ramp})
Number of Qubits (N)
Error = 5%
Error = 10%
Error = 20%
Error = 30%
2.8 log N-3.16
0
1
2
3
4
5
6
7
8
9
10
11
12
13
14
15
16
17

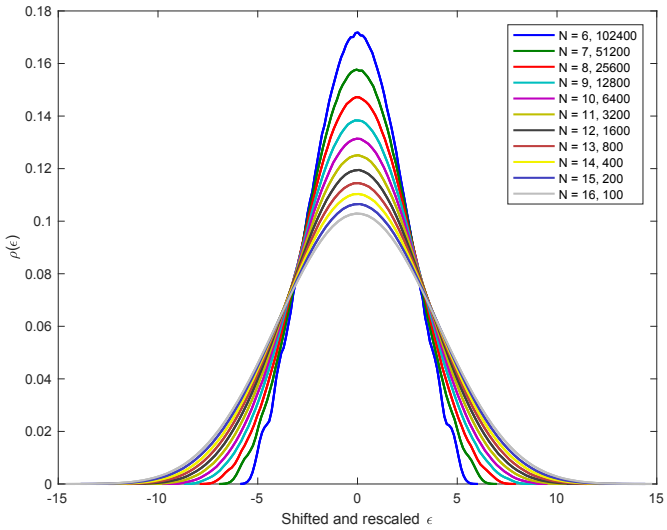
0.18
0.16
0.14
0.12
0.1
0.08
0.06
0.04
0.02
0
-15
-10
-5
0
5
10
15
$\rho(\epsilon)$
Shifted and rescaled ϵ
N = 6, 102400
N = 7, 51200
N = 8, 25600
N = 9, 12800
N = 10, 6400
N = 11, 3200
N = 12, 1600
N = 13, 800
N = 14, 400
N = 15, 200
N = 16, 100

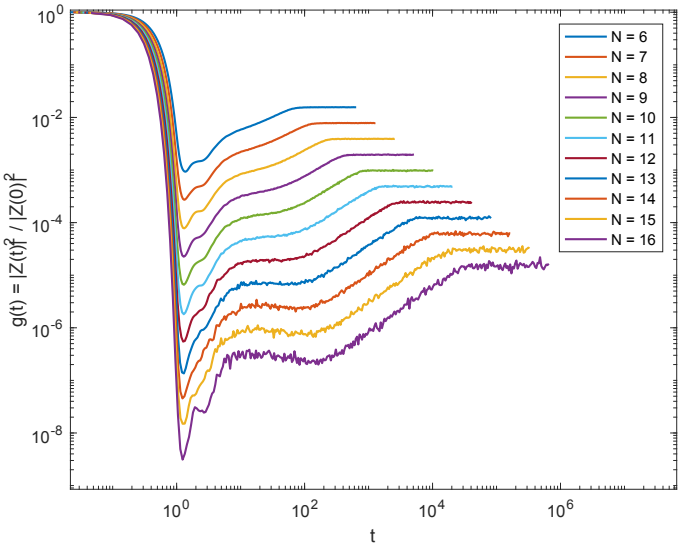
10^0
10^{-2}
10^{-4}
10^{-6}
10^{-8}
$g(t) = |Z(t)|^2 / |Z(0)|^2$
10^0
10^2
10^4
10^6
t
N = 6
N = 7
N = 8
N = 9
N = 10
N = 11
N = 12
N = 13
N = 14
N = 15
N = 16

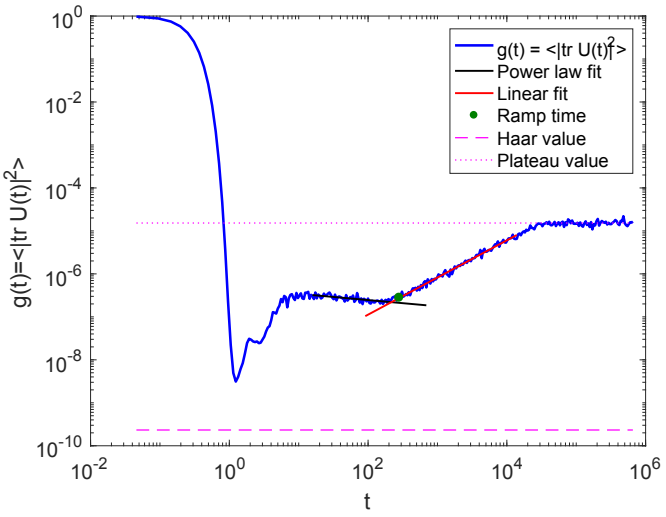
g(t) = <|tr U(t)|^2>
Power law fit
Linear fit
Ramp time
Haar value
Plateau value
g(t)=<|tr U(t)|^2>
t
10^0
10^-2
10^-4
10^-6
10^-8
10^-10
10^-2
10^0
10^2
10^4
10^6

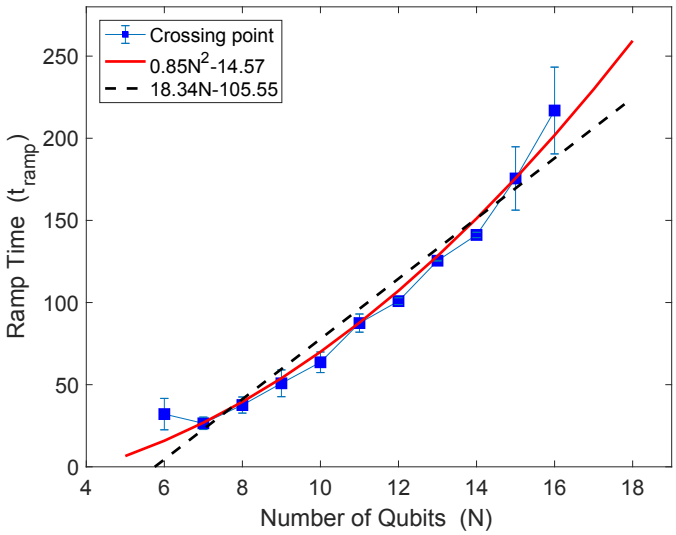
Crossing point
0.85N2-14.57
18.34N-105.55
Ramp Time (tramp)
Number of Qubits (N)
0
50
100
150
200
250
4
6
8
10
12
14
16
18

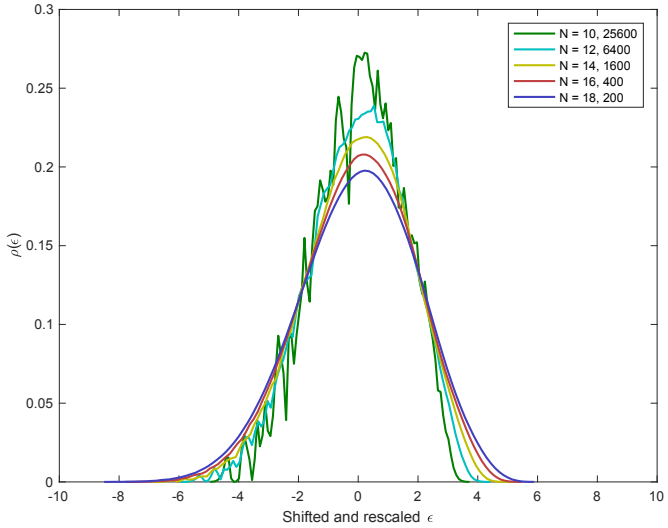
N = 10, 25600
N = 12, 6400
N = 14, 1600
N = 16, 400
N = 18, 200
$\rho(\epsilon)$
Shifted and rescaled ϵ
0.3
0.25
0.2
0.15
0.1
0.05
0
-10
-8
-6
-4
-2
0
2
4
6
8
10

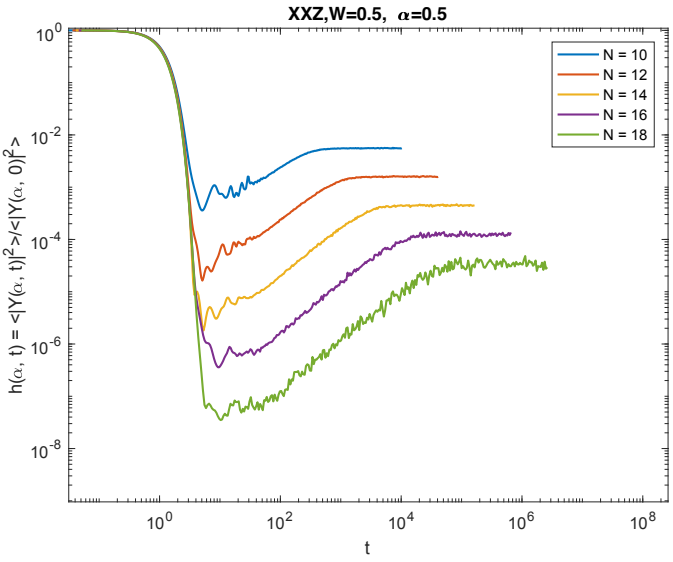
XXZ,W=0.5, α=0.5
N = 10
N = 12
N = 14
N = 16
N = 18
h(α, t) = <|Y(α, t)|²>/<|Y(α, 0)|²>
t
10^0
10^-2
10^-4
10^-6
10^-8
10^0
10^2
10^4
10^6
10^8

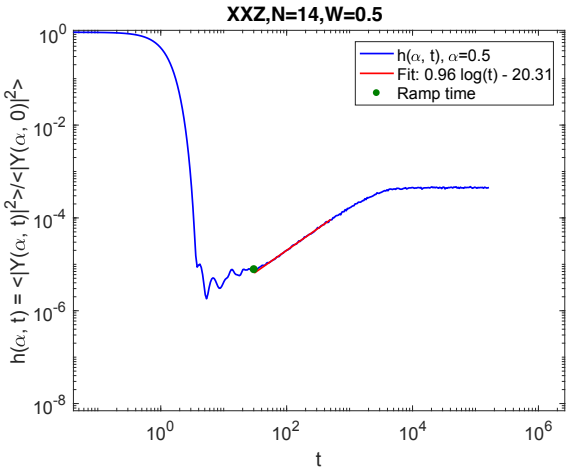
XXZ,N=14,W=0.5
h(α, t), α=0.5
Fit: 0.96 log(t) - 20.31
Ramp time
h(α, t) = <|Y(α, t)|^2>/<|Y(α, 0)|^2>
t

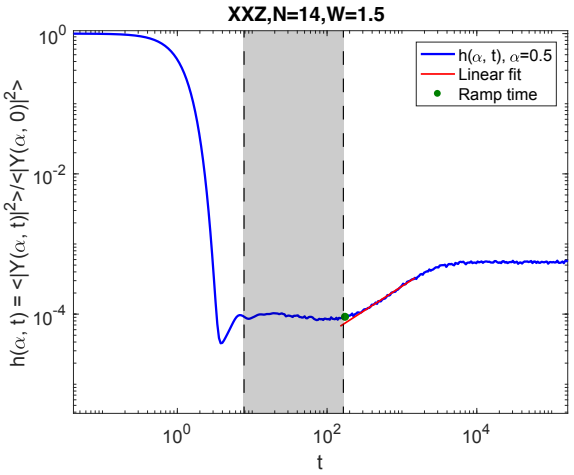
XXZ,N=14,W=1.5
h(α, t), α=0.5
Linear fit
Ramp time
h(α, t) = <|Y(α, t)|^2>/<|Y(α, 0)|^2>
t

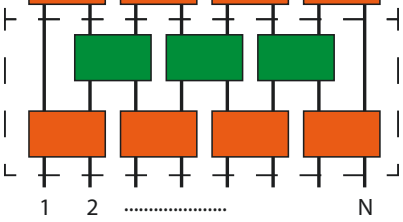
1 2 N

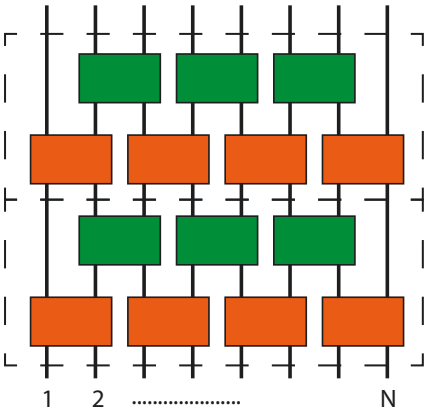
1 2 N

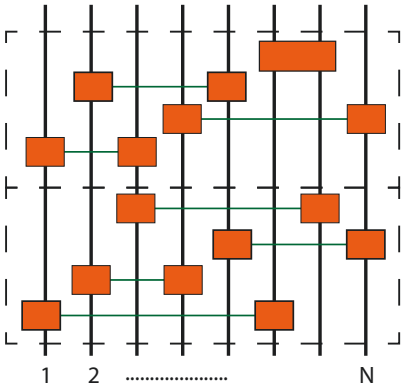
1 2 N

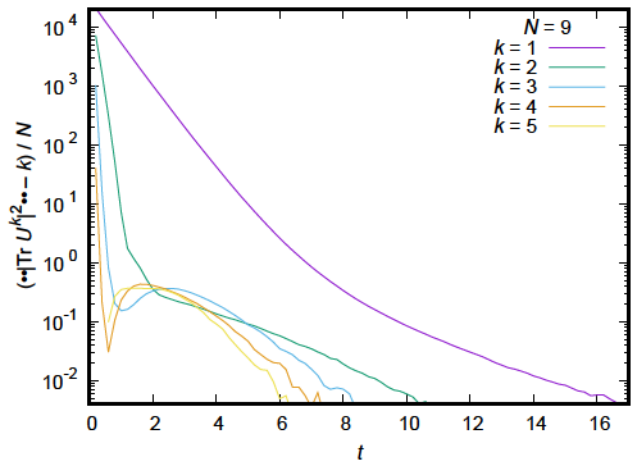

Figure 17: Plot of $(\langle|\mathrm{Tr}U^k|^2\rangle - k)/N$ for $k = 1, 2, 3, 4, 5$ against t for the 2-local RCQ chain with $dt = 0.2$. $N = 9$, 10^5 samples. These exhibit exponential decays with rates that do not decrease as k increases.

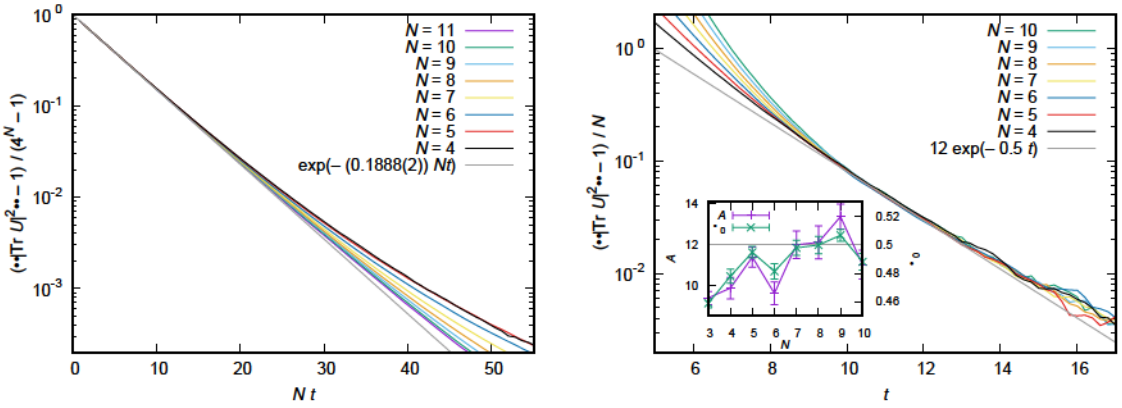

Figure 18: [Left] Plot of $(\langle|\mathrm{Tr}U|^2\rangle - 1)/(4^N - 1)$ against Nt for the RCQ chain with $dt = 0.2$ for $N = 11, 10, 9, 8, 7, 6, 5, 4$ qubits. The result of a single parameter fit by an exponential function of Nt is also shown. [Right] Plot of $(\langle|\mathrm{Tr}U|^2\rangle - 1)/N$ against t for the RCQ chain with $dt = 0.2$ for $N = 10, 9, 8, 7, 6, 5, 4$ qubits. The inset shows the result of fit for $t \in [10 : 14]$ with $Ae^{-\Delta_0 t}$ by taking A and Δ_0 as fitting parameters. The line corresponding to $(A, \Delta_0) = (12, 0.5)$ is also shown in the main plot.

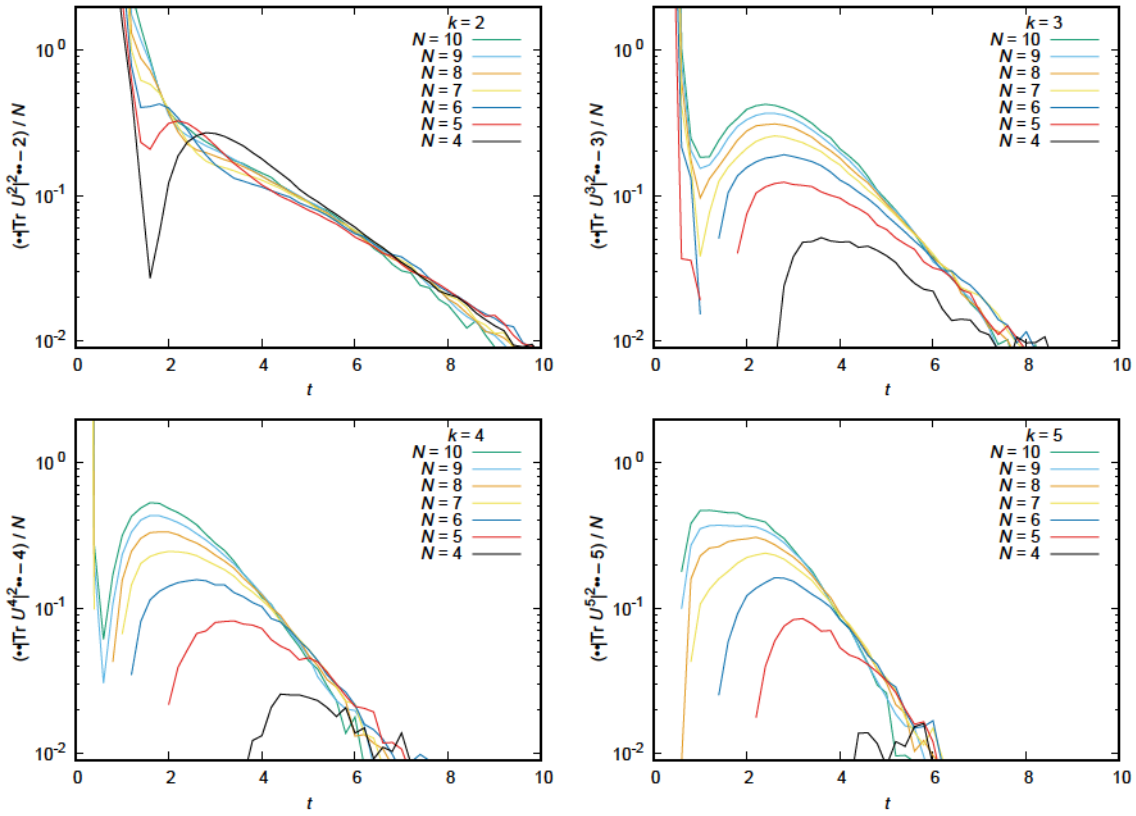

Figure 19: Plot of $(\langle|\mathrm{Tr}U^k(\tilde{t})|^2\rangle - k)/N$ against t for various values of N, $k = 2, 3, 4, 5$.

increases with k (see also Fig. 17)[26], which means the convergence to the Haar values at larger k happens earlier. Therefore, after t_{Haar} is determined from $k = 1$, higher moments have already converged.

Local RCQ Brownian circuit

Next we consider the Brownian circuit made from the local RCQ Hamiltonian introduced in Sec. 4.2.1. We expect the same decay pattern as in the 2-local RCQ. We have used the same number of samples as in the 2-local RCQ Brownian circuit case.

As shown in the left panel of Fig. 21, the early-time decay can be fit by $(\langle|\mathrm{Tr}U(t)|^2\rangle - 1) \simeq (4^N - 1) \cdot e^{-c(N-1)t}$ where $c \simeq 0.187$. Therefore, the early-time decay to $\langle|\mathrm{Tr}U(t)|^2\rangle - 1 \sim O(1)$ takes place within order one time. As shown in the right panel of Fig. 21 and in Fig. 22, the late time decay appears to be consistent with $\tilde{c}Ne^{-\Delta_k t}$ for $k = 1, 2, 3, 4$ and

[26] Δ_1 actually is approximately the same as Δ_2.

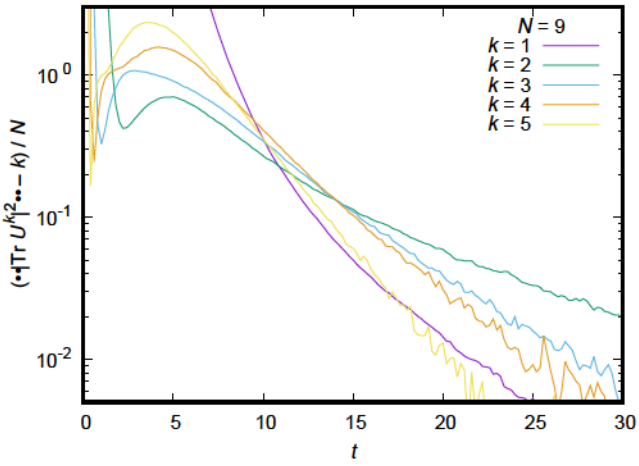

Figure 20: Plot of $\langle |\mathrm{Tr}U^k|^2\rangle - k$ for $k = 1, 2, 3, 4, 5$ for the local RCQ chain with $dt = 0.2$ for $N = 9$ qubits. The decay time scale appears to grow with k for $k \geq 2$.

5, where $\tilde{c}$ is an order one constant. These observations are the same as the case of the 2-local Brownian circuit. Note that here Δ_1 is larger than Δ_2. This is not surprising given the analysis above which shows they result from somewhat different mechanisms. But for $k > 2$, $\Delta_k > \Delta_2$ indicating that $k = 2$ is already in the stable range for determining the approach to random matrix behavior.

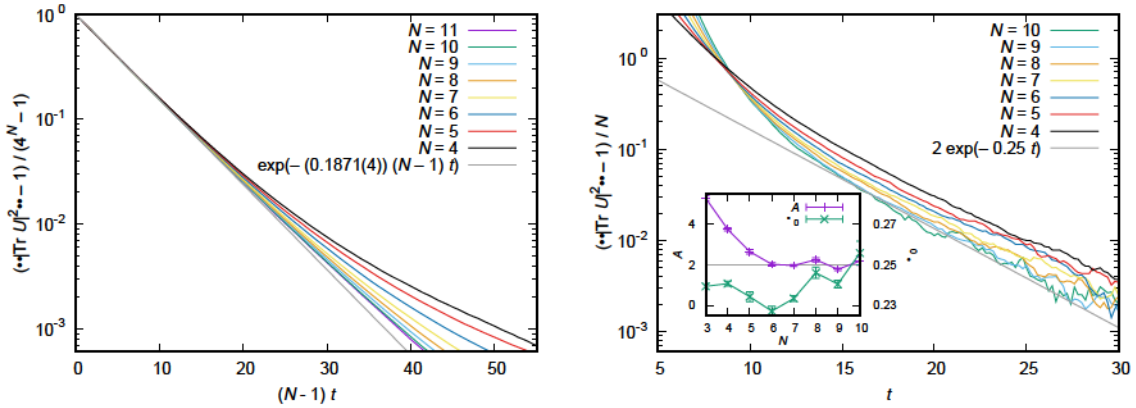

Figure 21: [Left] Plot of $(\langle|\mathrm{Tr}U|^2\rangle - 1)/(4^N - 1)$ against $(N-1)t$ for the local RCQ chain with $dt = 0.2$ for $N = 11, 10, 9, 8, 7, 6, 5, 4$ qubits. [Right] Plot of $(\langle|\mathrm{Tr}U|^2\rangle - 1)/N$ for the local RCQ chain with $dt = 0.2$ for $N = 10, 9, 8, 7, 6, 5, 4$ qubits.

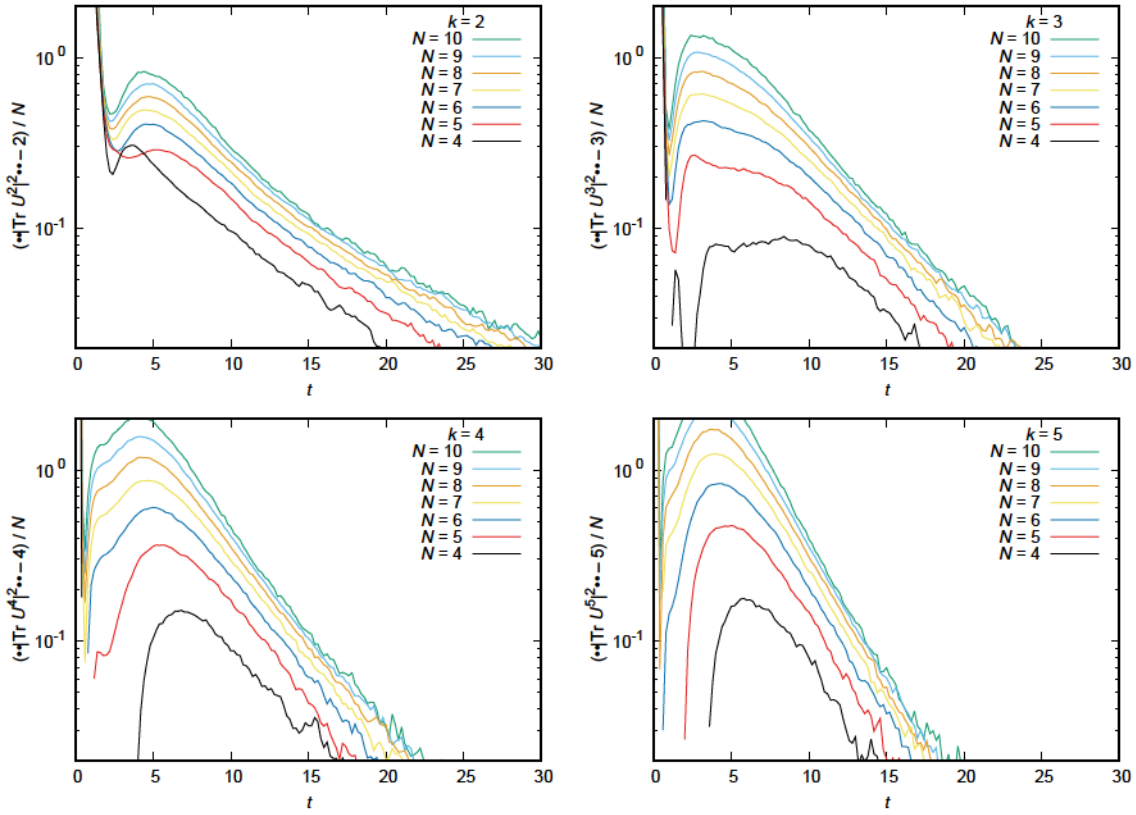

Figure 22: Plot of $(\langle|\mathrm{Tr}U^k|^2\rangle - k)/N^2$ against t for the local RCQ chain with $dt = 0.2$ for $N = 10, 9, 8, 7, 6, 5, 4$ qubits, $k = 2, 3, 4, 5$. An exponential fit of the $N = 9$ curve is also shown.

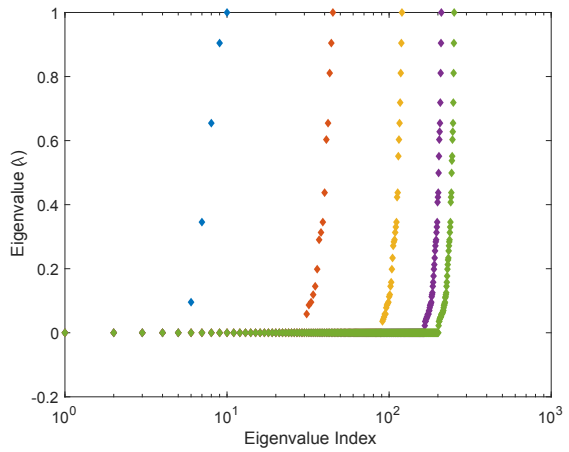
Eigenvalue (λ)
Eigenvalue Index

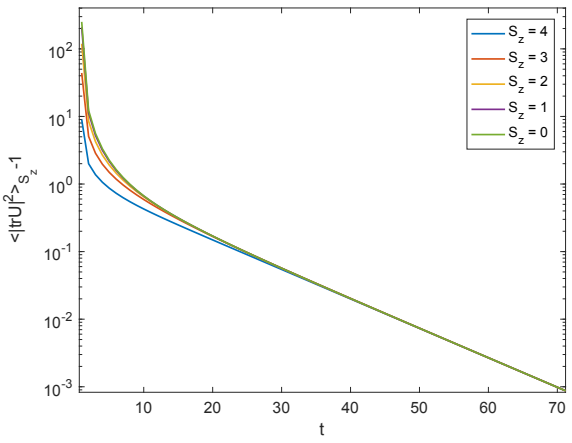
S_z = 4
S_z = 3
S_z = 2
S_z = 1
S_z = 0
<|trU|^2>_Sz^-1
t

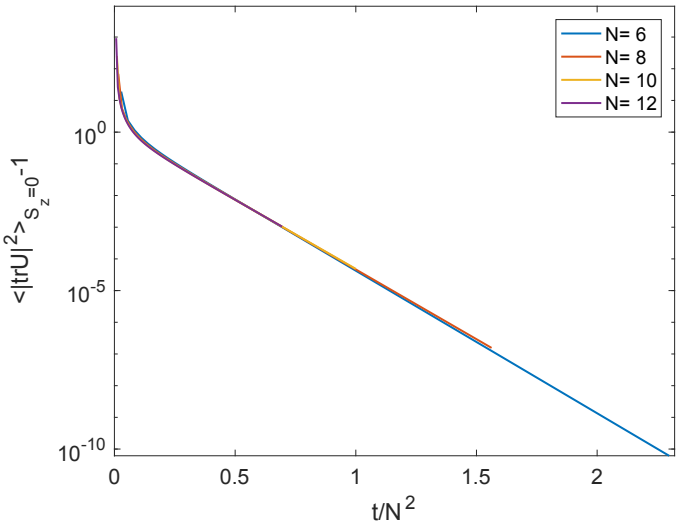
N= 6
N= 8
N= 10
N= 12
<|trU|^2>_Sz=0^-1
t/N^2

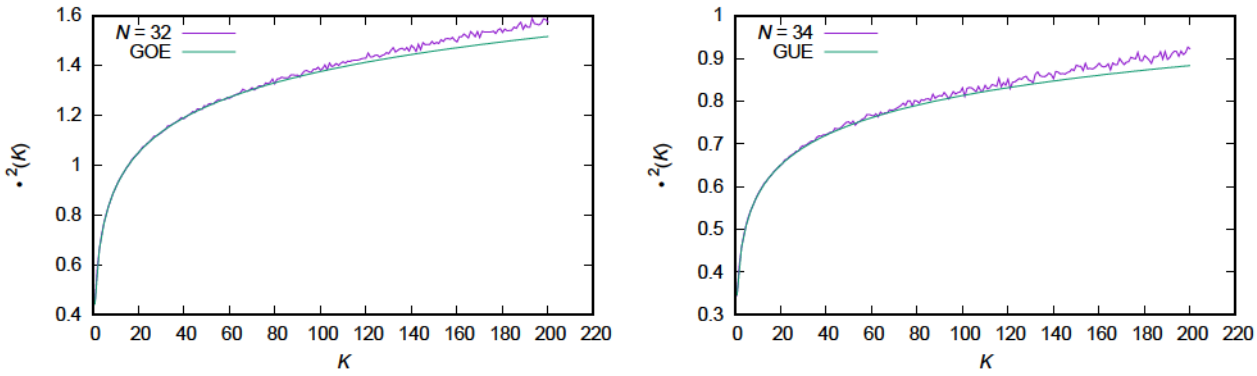

Figure 24: $\Sigma^2(K)$ for the SYK model, $N = 32$ (250 samples) and $N = 34$ (110 samples), obtained using the unfolded spectra after shifting and rescaling. The curves for corresponding random matrix ensembles, GOE and GUE, are also plotted.

4. Then we compute $\Sigma^2(K)$.

Steps (1) and (2) are not implemented in [7]. The number variance calculated in this manner is shown in Fig. 24, for $N = 32$ and $N = 34$. The agreement with RMT persists to larger K, roughly a factor of two larger, than in [7]. Thus we see that the number variance is sensitive to the unfolding procedure.

As discussed in the text we expect that RMT behavior extends to an exponentially large value of K, much larger than shown even by these improved results. Our unfolding procedure is still rather crude. As a first step one could try to fully unfold the spectrum sample by sample. But it is unclear to us whether this is even in principle sufficient. At a minimum an exponentially large number of samples would be required to get a sufficiently accurate value of the variance.

For this reason the number variance seems not to be the best quantity to probe long range spectral rigidity in many-body systems. As discussed in the text the spectral form factor is less sensitive to such errors.

A.2 Estimating t_{min} in the SYK Model

In this appendix we give our detailed results for determining t_{min} in the SYK model numerically. The algorithm used to select an optimal α is as follows: In the second panel of Figure 3 we have varied α with step size 0.5, and observed that some α between $2.5 < \alpha < 3.0$ gives the smallest value of t_{min}; at $\alpha \leq 2.5$ the oscillation due to the sharp

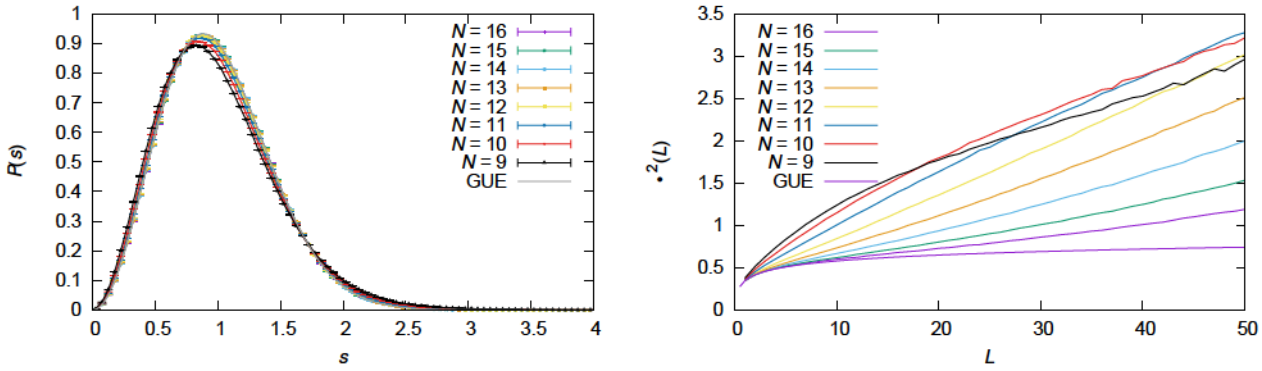

Figure 25: Unfolded level separation distribution $P(s)$ for the RCQ model for $N = 9, 10, \ldots, 16$ compared against the Padé approximant for GUE, and the number variance $\Sigma^2(K)$. L on the right panel corresponds to K in the text.

A.3 Eigenvalue Behavior for 2-local RCQ

In order to test the spectral rigidity of the energy spectrum, we performed the unfolding with steps $1-4$ explained in Sec. A.1. The shifted-and-rescaled energy spectrum (obtained by performing steps 1, 2 and 3), before the unfolding, is shown in the right panel of Fig. 5. Unlike the SYK model, the edge of the spectrum is not sharp. Due to this, the slope of SFF decays much faster, as we will see shortly. The nearest-level separation obtained from the unfolded spectrum is plotted in the left panel of Fig. 25. A good agreement with GUE ensemble at large N can be seen. The number variance $\Sigma^2(K)$ is plotted in the right panel of Fig. 25. At $N = 16$, an agreement with RMT can be seen only at $K \lesssim 10$.

B Analytic Results for Random Quantum Circuit

In this appendix we collect several analytic results which complement the discussion in Sec. 5.

B.1 k-th Moment of the Haar Measure

If we take the average with respect to the Haar measure on $\mathrm{U}(L)$, $u(k,t) = \left\langle |\mathrm{Tr}U^k(t)|^2 \right\rangle$ is equal to k for $k \leq L$ and is equal to L for $k > L$. For $k = 1$ and $k = 2$, it can be seen

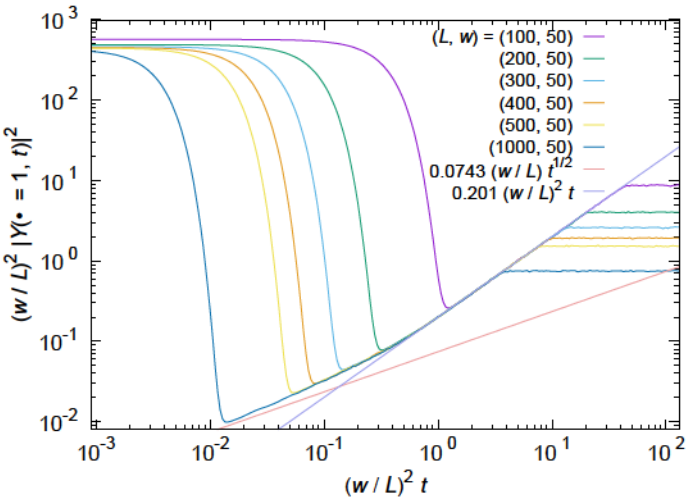

Figure 26: $(w/L)^2|Y(\alpha = 1, t)|^2$ vs $(w/L)^2 \cdot t$, $L = 100, 200, 300, 400, 500, 1000$, $w = 50$, $\alpha = 1$. 10000 samples have been taken.

Hilbert space, which connects w nearby states. This looks 'local' if we identify the states with a single particle hopping on L lattice sites, but it is useful to note that this is rather different from a many-body local Hamiltonian, say a local spin system. In the latter, in a natural local basis, the Hamiltonian is sparse but the nonzero entries are not aligned near the diagonal as in the banded matrix.

In local Hamiltonians with N spins, each row and column has $L = 2^N$ entries, among which there are $O(N)$ nonzero elements. This is much sparser than a banded matrix with $w \sim \sqrt{L}$, but it can already be chaotic. The time scales are also very different; the ramp time for the local Hamiltonian, $t_{\text{ramp}} \sim N^2 \sim (\log L)^2$ (see Sec. 4.2), is much shorter than $(L/w)^2$ when $w \sim \sqrt{L}$.

C.2 Brownian Circuit

The Brownian circuit of random band matrices can describe diffusion, because the number of particles — which is one — is conserved. For this reason, as we will see, we can confirm $t_{\text{Haar}} \sim (L/w)^2 \sim t_{\text{diff}}$.

The numerical procedure is the same: we calculate $U(t) = \prod_{k=1}^{n} e^{-iH_k dt}$, where $t = n \cdot dt$ and H_k are $L \times L$ random band matrices with a width w. From this we calculate the $\langle |TrU|^2 \rangle$.

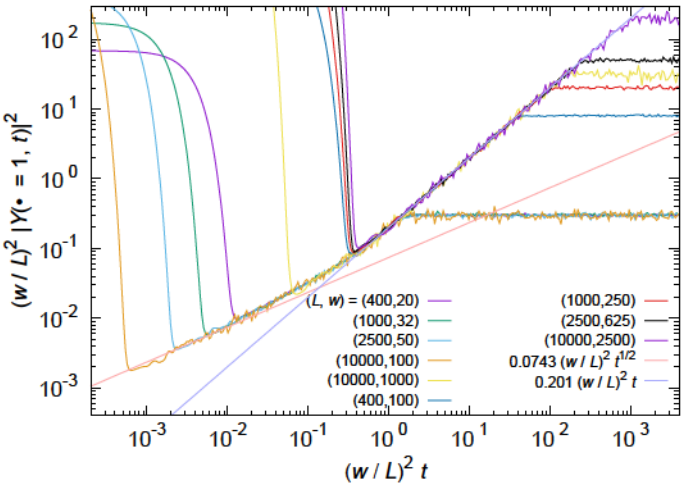

Figure 27: The value of $(w/L)^2|Y(\alpha=1,t)|^2$ plotted against $(w/L)^2\cdot t$ for various (L,w) satisfying $\sqrt{L}\le w\le L/4$, $\alpha=1$. The number of samples with each value of w is $10^6/L=2500,1000,400,100$ for $L=400,1000,2500,10000$ cases. For $w\ll L/4$ the initial growth indicates that $|Y(\alpha=1,\tau)|^2\sim(L/w)\sqrt{t}$, while for all (L,w) plotted, the growth for larger t before the plateau agrees with $|Y(\alpha=1,t)|^2\sim t$.

First let us see that the specific choice of dt is not important. When dt is sufficiently small, if we take $tdt=n(dt)^2$ to be the horizontal axis, the dt-dependence is gone; see Fig. 29. This scaling can be understood if the time evolution is described as a random walk with step-size wdt. After n steps, the typical distance from the starting point should be $\sqrt{n}wdt$, if the random walk picture is true. Then for fixed L and w the dt-dependence should disappear when the horizontal axis is $n(dt)^2$. Below we fix dt to be 0.5.

In Fig. 28 we have plotted $\langle|\mathrm{Tr}U|^2\rangle-1$ against $(t(w/L)^2)/(L^2-1)$ for fixed $w=25$ and various L, and for a fixed L/w. In both cases we can see an exponential decay. The exponent is a function of L/w, as we can see from the right panel of Fig. 28.

As we can see from Fig. 30, we can show the exponential decay at late time as well, $\langle|\mathrm{Tr}U|^2\rangle-1\sim e^{-2t(w/L)^2}$. Note that the exponent is different from the early time. If we define t_{Haar} as the time $\langle|\mathrm{Tr}U|^2\rangle-1$ reaches to a certain value, say 0.1, then this scaling leads to $t_{\mathrm{Haar}}\sim(L/w)^2$.

It is possible to understand this scaling from the random walk picture. When the average distance from the starting point, which is $\sqrt{t}w$, is of order L, it is natural to expect that the transfer matrix U is almost a random unitary. Therefore $\sqrt{t_{\mathrm{Haar}}}w\sim L$, or

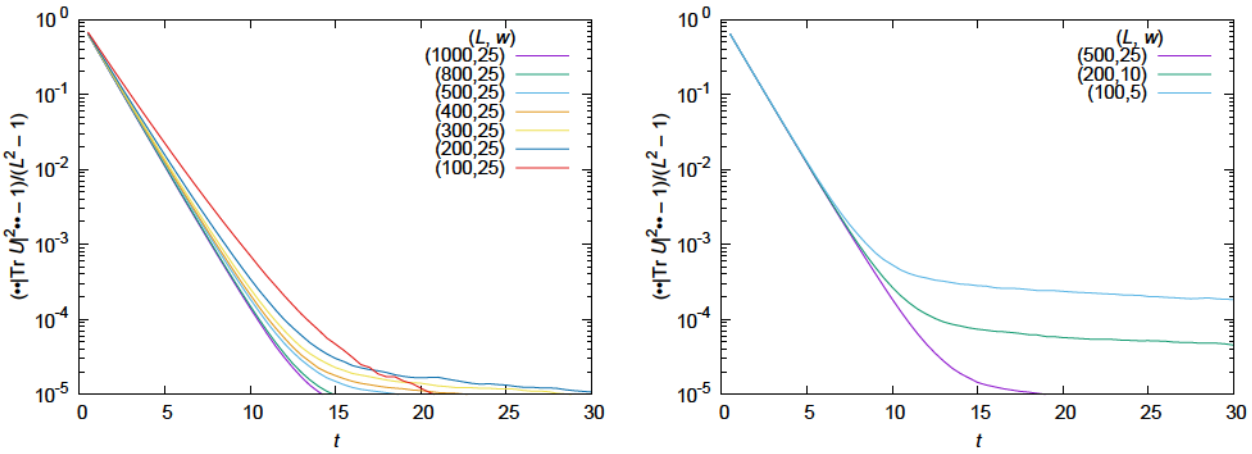

Figure 28: Plot of $(\langle|\mathrm{Tr}U|^2\rangle - 1)/(L^2-1)$ against t for $w = 25$ and various values of L (left) and for $L/w = 20$ with $L = 500, 200, 100$ (right). $dt = 0.5$ is fixed.

equivalently, $t_{\mathrm{Haar}} \sim (L/w)^2$.

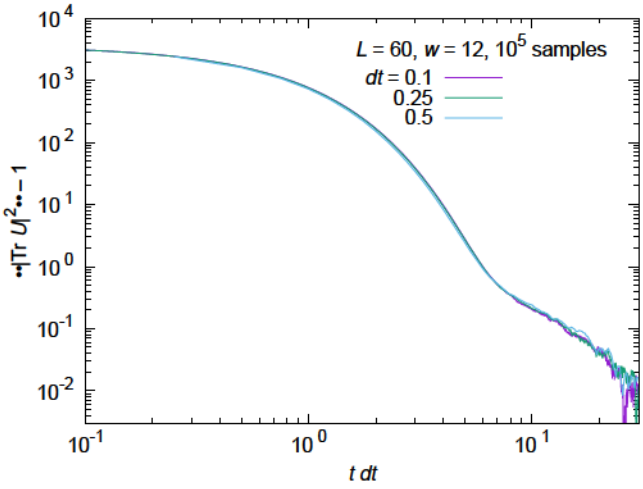

Figure 29: Plot of $\langle|\mathrm{Tr}U|^2\rangle - 1$ against $t\ dt$ for $dt = 0.1, 0.25, 0.5$ for Brownian circuits of random band matrices with $L = 60$ and $w = 12$. 10^5 samples have been taken for each choice of dt.

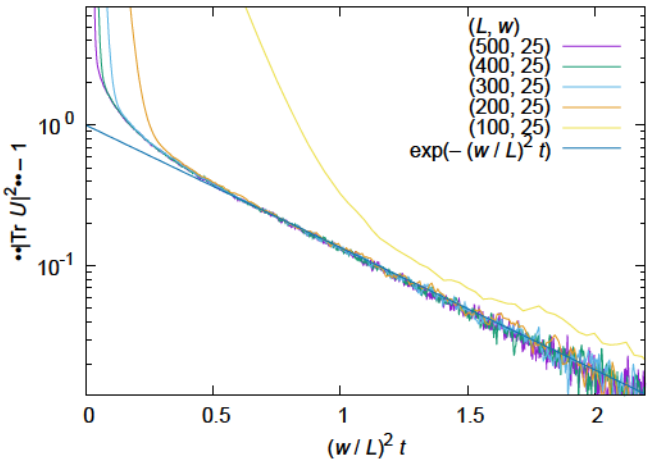

Figure 30: Log plot of $\langle|\mathrm{Tr}U|^2\rangle - 1$ against $t(w/L)^2$ for $w = 25$ and various values of L. $dt = 0.5$ is fixed. 10^5 samples have been used for $L = 300, 200, 100$.

Springer-Verlag New York, Inc.

Phys. Rev. B 10.1103/PhysRevB.93.041424

arXiv:1712.05073 [cond-mat.str-el]

arXiv:1803.03841 [cond-mat.stat-mech]

$\hbar$

arXiv:1712.02665 [nlin.CD]

Phys. Rev. B
doi:10.1103/PhysRevB.95.115150 arXiv:1602.06964 [cond-mat.str-el]

Phys. Rev. D
arXiv:1610.03816 [hep-th]

doi:10.1007/JHEP05(2017)118 arXiv:1611.04650 [hep-th]

Phys. Rev. Lett. arXiv:cond-mat/9212030
[cond-mat]

Talk 1 Talk 2

arXiv:1711.08467 [hep-th]

Phys. Rev. arXiv:1604.07818 [hep-th]

Sov. Phys. JETP

JHEP arXiv:0708.4025 [hep-th]

JHEP 0810, 065 (2008) arXiv:0808.2096 [hep-th]

JHEP , 018 (2013)

Fundamental Physics Prize Symposium

JHEP arXiv:1111.6580 [hep-th]

JHEP arXiv:1306.0622 [hep-th]

doi:10.1007/JHEP12(2014)046

doi:10.1007/JHEP03(2015)051

JHEP arXiv:1412.6087 [hep-th]

JHEP arXiv:1503.01409 [hep-th]

Sov. Phys. JETP

Comm. Math. Phys.
10.1007/s00220-014-2119-5

arXiv:1801.01071
[hep-th]

Nucl. Phys. B
doi:10.1016/0550-3213(84)90184-6

Phys. Rev. A arXiv:0503210 [quant-ph]

Phys. Rev. Lett., 98(130502) arXiv:0605126 [quant-ph]

Science

J. Math. Phys. arXiv:0611002 [quant-ph]

Phys. Rev. A arXiv:0807.0775 [quant-ph]

Proc. of APPROX-RANDOM *LNCS*
arXiv:0811.2597

Comm.Math.Phys. arXiv:0802.1919 [quant-ph]

Phys. Rev. Lett. arXiv:0910.0913 [quant-ph]

arXiv:1210.6644 [quant-ph]

arXiv:1208.0692 [quant-ph]

Commun. Math. Phys. doi:10.1007/s00220-017-2950-6 arXiv:1606.01914[quant-ph]

Phys. Rev. X arXiv:1609.07021

Phys. Rev. X arXiv:1704.03041

arXiv:1705.08975[cond-mat.str-el]

arXiv:1705.08910 [cond-mat.str-el]

arXiv:1710.09835 [cond-mat.stat-mech]

arXiv:1203.5813

arXiv:1709.06678

Nature

arXiv:1803.04402

arXiv:1710.09827 [cond-mat.stat-mech]

arXiv:1610.04903 [quant-ph]

JHEP 1706.05400 [hep-th]

J. Math. Phys.

Random matrices

Phys. Rept. arXiv:9707301 [cond-mat]

Phys. Rev. E arXiv:0006144 [cond-mat]

arXiv:1712.05073 [cond-mat.str-el]

Mathematical Physics, Analysis and Geometry

arXiv:1407.1552 [math-ph]

Physical Review E cond-mat/9608116

Phys. Rev.

Phys. Rev. Lett. arXiv:1502.06692 [hep-th]

1706.07439 [hep-th]

Nucl. Phys. B

doi:10.1016/j.nuclphysb.2016.08.002 1607.00694 [cond-mat.str-el]

JHEP

doi:10.1007/JHEP10(2017)008 arXiv:1703.04612 [hep-th]

J. Phys. A: Math. Gen. ***32****, 6903 (1999)*

Trans. Am. Math. Soc.

Markov Processes and Related Fields arXiv:1403.1114 [math-ph]

Communications in Mathematical Physics arXiv:1403.1121 [math-ph]

arXiv:1003.2613 [ond-mat.dis-nn]

Phys. Rev. B

10.1103/PhysRevB.91.081103

Annalen der Physik 529 arXiv:1611.00770 [cond-mat.dis-nn]

Comput. Phys. arXiv:cond-mat/9809162

J. Phys. A: Math. Theor.

arXiv:1207.4106 [cond-mat.stat-mech]

Commun. Math. Phys. doi:10.1007/BF01645779

arXiv:1802.02633 [hep-th]

Phys. Rev. Lett.